Enhanced coupling of light into a turbid medium through microscopic interface engineering

Jonathan V. Thompson[a], Brett H. Hokr[a], Wihan Kim[b], Charles W. Ballmann[a], Brian E. Applegate[b], Javier Jo[b], Alexey Yamilov[c], Hui Cao[d], Marlan O. Scully[a,e,1], and Vladislav V. Yakovlev[b]

[a]Institute for Quantum Science and Engineering, Texas A&M University, College Station, TX 77843; [b]Department of Biomedical Engineering, Texas A&M University, College Station, TX 77843; [c]Department of Physics, Missouri University of Science & Technology, Rolla, MO 65409; [d]Department of Applied Physics, Yale University, New Haven, CT 06520; and [e]Department of Physics, Baylor University, Waco, TX 76798

Contributed by Marlan O. Scully, June 16, 2017 (sent for review April 4, 2017; reviewed by Vanderlei S. Bagnato and Shiyao Zhu)

There are many optical detection and sensing methods used today that provide powerful ways to diagnose, characterize, and study materials. For example, the measurement of spontaneous Raman scattering allows for remote detection and identification of chemicals. Many other optical techniques provide unique solutions to learn about biological, chemical, and even structural systems. However, when these systems exist in a highly scattering or turbid medium, the optical scattering effects reduce the effectiveness of these methods. In this article, we demonstrate a method to engineer the geometry of the optical interface of a turbid medium, thereby drastically enhancing the coupling efficiency of light into the material. This enhanced optical coupling means that light incident on the material will penetrate deeper into (and through) the medium. It also means that light thus injected into the material will have an enhanced interaction time with particles contained within the material. These results show that, by using the multiple scattering of light in a turbid medium, enhanced light–matter interaction can be achieved; this has a direct impact on spectroscopic methods such as Raman scattering and fluorescence detection in highly scattering regimes. Furthermore, the enhanced penetration depth achieved by this method will directly impact optical techniques that have previously been limited by the inability to deposit sufficient amounts of optical energy below or through highly scattering layers.

turbid media | enhanced transmittance | optical coupling | optical scattering | spectroscopy

Optical detection and spectroscopy has drastically changed the way we look at and measure the world today. Observation of the interaction of light with matter provides us with a host of tools to promote research, security, safety, and health. These optical tools include the detection of harmful or explosive materials (1–3), the remote detection of chemicals from a distance (4), the optical diagnosis of colloidal suspensions for genomics and drug delivery (5), and even the use of lasers for defense (6). Remote sensing techniques (7) allow us to image/detect structures through the atmosphere or ocean. Optical methods are also an integral part of biomedical research, diagnosis (8), and treatment (9) of many of today's most prevalent illnesses (10). However, the sensitivity and usefulness of any optical method is severely limited by the occurrence of optical scattering. This limitation is further amplified when the density of scatterers is high enough for multiple scattering to occur. In this article, we show that modification of the geometry of the optical interface significantly improves the coupling efficiency of light into a highly scattering medium, thereby reducing the detrimental effects of scattering. This enhanced coupling is evident through the observation of increased spatial diffusion, two orders of magnitude greater transmission, and over an order of magnitude greater interaction time of light within the material. This translates to over an order of magnitude greater sensitivity for linear optical detection methods such as spontaneous Raman scattering or fluorescence. Thus, by using the multiply scattering nature of a material, we can substantially increase the effectiveness and sensitivity of optical methods in and through turbid media. These results may also impact technologies such as random lasing (11), optical systems on a chip (12, 13), and photon management in films and solar cells (14, 15).

When light is incident upon a disordered, highly scattering material, the injection depth and optical path length of the light within the medium is limited by its scattering properties (16). Thus, light–matter interactions are confined to regions near the optical entrance, as shown in Fig. 1, *Left*. One way to circumvent the scattering at the surface of a material is to physically insert an optical needle probe (17) into the material and deposit/collect light directly at the location of interest; however, physical access to the scattering material is not always possible.

Other ways to overcome inefficient coupling of light into scattering materials have included the use of wavefront shaping (18–20) to promote coupling into the fundamental diffusion mode (21) or the open/closed eigenchannels (22, 23) of the material, thereby controlling energy density (13). An optimum wavefront of the incident light is determined via iterative search algorithms (24, 25) or measurement of the transmission/reflection matrix (26) to promote coupling into these modes. In practice, the sample must remain static for the entire measurement procedure, which may require seconds to minutes of time to complete. Some of the limitations of wavefront shaping, namely, the incomplete channel control of the input light, measurement noise in the optimization algorithm, and measurement time, have been avoided by placing the scattering material inside a waveguide with an engineered geometry (27). Although the control of light coupling into the scattering material was achieved without wavefront shaping, each sample required a custom-built waveguide to greatly enhance energy

Significance

Optical scattering severely limits the range and sensitivity of detection techniques within/through turbid media, such as biological samples and security-related materials. In this article, we demonstrate a method to enhance the coupling of light into a highly scattering medium. This enhanced coupling results in higher optical sensitivity to particles within the medium, as well as enhanced optical transmission through the medium. These results pave the way for enhanced spectroscopy in biological and other turbid media.

Author contributions: J.V.T., B.H.H., B.E.H., J.J., M.O.S., and V.V.Y. designed research; J.V.T., B.H.H., W.K., C.W.B., and B.E.A. performed research; J.V.T., B.H.H., A.Y., H.C., and V.V.Y. contributed new reagents/analytic tools; J.V.T. and B.H.H. analyzed data; and J.V.T. wrote the paper.

Reviewers: V.S.B., University of Sao Paulo; and S.Z., Beijing Computational Science Research Center.

The authors declare no conflict of interest.

[1]To whom correspondence should be addressed. Email: scully@tamu.edu.

This article contains supporting information online at www.pnas.org/lookup/suppl/doi:10.1073/pnas.1705612114/-/DCSupplemental.

Downloaded at Palestinian Territory, occupied on December 11, 2021

PHYSICS

APPLIED BIOLOGICAL SCIENCES

www.manaraa.com

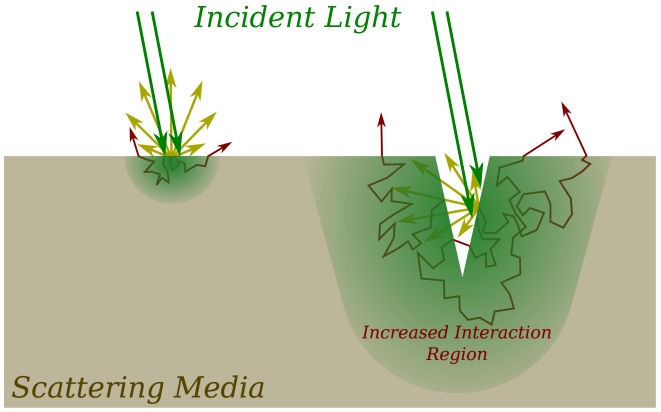

Fig. 1. (*Left*) When light is scattered by a highly turbid material, the majority of the light is scattered in all directions near the surface. If the surface geometry of the material is such that the light scattered near the surface is directed toward another surface, the likelihood of the light scattering into the material increases. (*Right*) A geometry such as that depicted would provide light rays with many scattering events before it escapes. This configuration greatly improves the chance that light will be injected deeper into the material, thereby enhancing the interaction region of light with the material.

delivery deep inside the random medium. Other methods include the use of an ultrasonic guide star and optical phase conjugation (28) for enhanced focusing of light in a turbid medium. Plasmonic or photonic structures with nanoscale fabrication have also been used to demonstrate enhanced optical coupling (14) or transmission (29).

In this article, we demonstrate an approach to achieve substantially enhanced coupling efficiency of light into a turbid medium via engineering of the optical interface at scales much larger than that required for plasmonic devices. Here, the interface modification is achieved via laser ablation. In the multiple scattering regime, the diffusion of light within a turbid medium is described by the optical diffusion equation for radiative transport (30, 31) (*Materials and Methods*). The penetration depth, and therefore the interaction region, of light within the material is limited by the transport mean free path, $l_t = 1/\mu_t$. Here, the extinction coefficient of the material, $\mu_t = \mu_s' + \mu_a$, is proportional to both the absorption (μ_a) and reduced scattering (μ_s') coefficients. The reduced scattering coefficient, $\mu_s' = (1 - g)\mu_s$, takes into account anisotropic scattering via the anisotropy parameter $g = \langle \cos(\theta) \rangle$, where θ is the scattering angle. Therefore, when light is incident upon a material with a large extinction coefficient, the shallow penetration depth confines light–matter interactions to regions near the injection point (Fig. 1). If, however, we inject the light past the top layer of the material (Fig. 1, *Right*), the scattering properties of the top layer will scatter more light back into the sample, effectively trapping, or coupling, the light inside the medium. As a result, the light will interact with the medium for longer periods of time and diffuse farther in all directions (including the forward direction) before escaping.

We show that this enhanced coupling can be realized by microscopic engineering of the geometry of the optical interface of a scattering medium. In particular, by focusing light into a narrow, conically shaped hole (0.3 mm deep) in the surface of a highly scattering material, we achieve an enhanced coupling of light into the material. This enhanced coupling is experimentally observed through the measurement of an increased diffusion radius of the backscattered light, an increased dwell time of light in the material (over an order of magnitude), and an increased transmission of light through the material (over two orders of magnitude). We also show that, as the depth of the narrow hole increases, this coupling can be further enhanced.

Results

A scattering sample with an engineered optical interface is constructed using laser ablation from a picosecond laser (Attodyne APL-X, 532 nm, 35 μJ) to drill a microscopic hole in the surface of a packed barium sulfate (243353; Sigma-Aldrich) sample. Barium sulfate has a transport mean free path of $l_t = 1.2$ μm ($\mu_t = 833.2$ mm^{-1}) as measured by coherent backscattering (32). Fig. 2 shows a hole in this material ablated with 250 laser pulses as measured by optical coherence tomography (OCT). The hole is about 300 μm deep, and has a diameter of about 100 μm at the surface. Because the hole is very narrow and deep, most of the light focused into it will have an increased likelihood of scattering, or coupling, into the sample.

The first indication of increased optical coupling is the observation of an enhanced diffusion radius in the backscattered light. Images acquired in the backward direction of light scattered from samples with and without a hole are shown in Fig. 3 *B* and *C*. As measured by these images, the intensity of the backscattered light near the focus of the laser decreases by a factor of 3.5 after the hole is drilled. By blocking the focus with a needle as in Fig. 3 *D* and *E*, we also see that more light is detected far away from the focus (radially) when the hole is present. In particular, the intensity of light 0.6 mm away from the focus is enhanced by over an order of magnitude when the light is focused into the hole. These two observations indicate that substantially more of the incident laser light is successfully injected into and diffuses farther inside the material with an engineered interface present.

The enhanced diffusion from improved optical coupling is also observed in the forward direction as enhanced transmission. To measure this, the intensity of light transmitted through a 1-cm-thick (10^4 transport mean free paths) sample was measured with a large area photodiode (DET100A; Thorlabs) for scenarios with the laser coupled and uncoupled into the hole in the sample. The transmittance of the light through the sample was measured to be 4×10^{-6} for the uncoupled case, and 9.6×10^{-4} for the coupled case. This is an increased transmission of over 200 times, even though the hole is only 3% of the total thickness of the sample. The back surface of the powder was imaged onto a CCD (CGE-B013-U; Mightex), and the images for both cases are shown in Fig. 3 *F* and *G*. Plotted in log scale, these images clearly show the drastic enhancement in optical penetration depth. Optical diffusion theory (30) (*Materials and Methods*) indicates that this enhanced transmission is not merely due to reduction of the

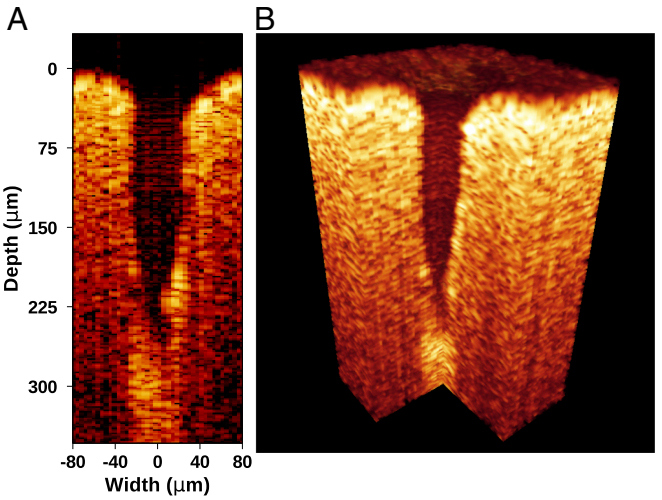

Fig. 2. (*A*) Cross-section and (*B*) 3D rendering of a scattering sample with a microscopic hole in the surface as measured by OCT. The laser-ablated hole is measured to be about 100 μm in diameter and 300 μm deep.

Downloaded at Palestinian Territory, occupied on December 11, 2021
www.manaraa.com

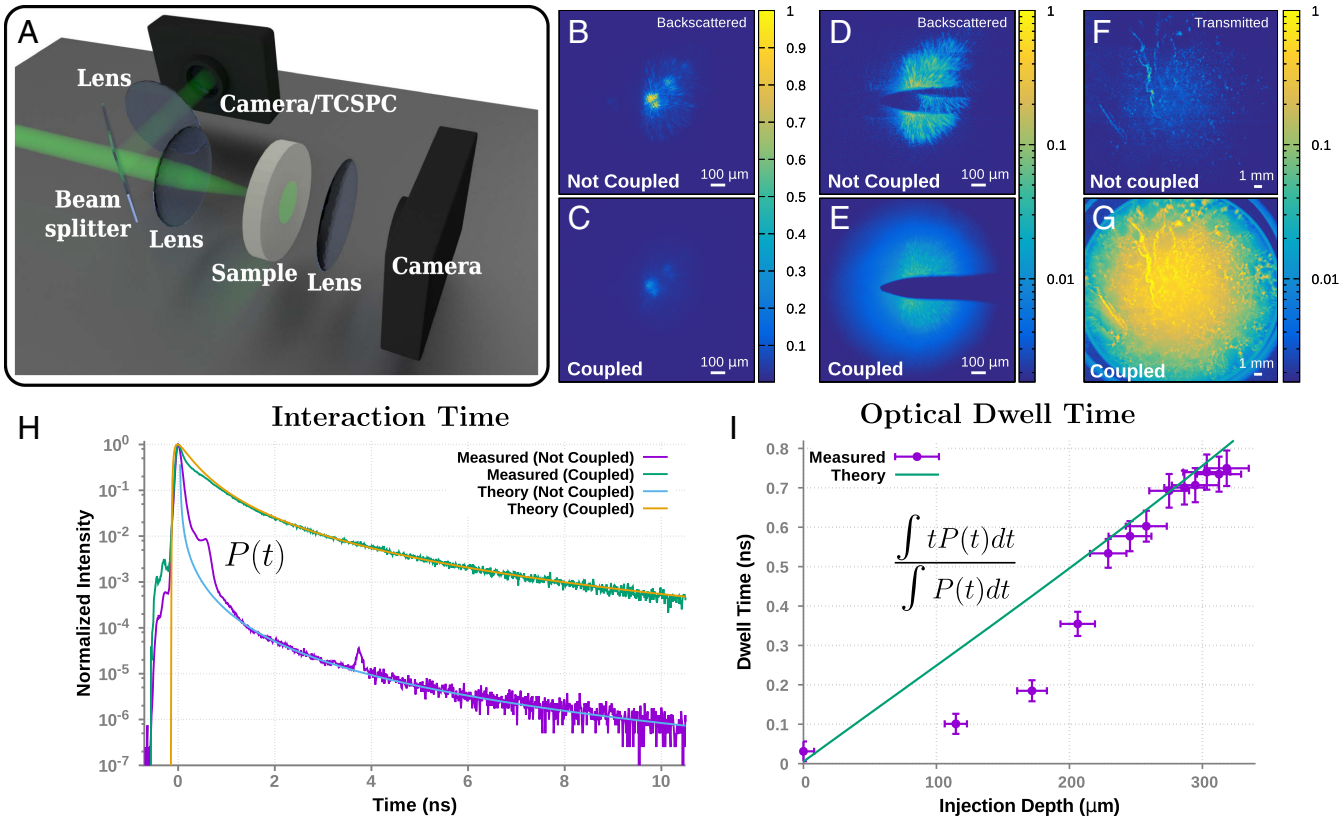

Fig. 3. Enhanced coupling of light into a scattering medium is observed via increased spatial diffusion, transmission, and dwell time, measured by detectors in the forward and backward directions (*A*). Backscattered light is imaged for (*C* and *E*) coupled and (*B* and *D*) uncoupled light. In *D* and *E*, a needle is used to block the bright focus, allowing observation of the enhanced spatial diffusion. Images of light transmitted through a 1 cm thick sample for (*G*) coupled and (*F*) uncoupled incident light shows two-orders-of-magnitude enhancement. (*H*) The normalized temporal profile of backscattered light also shows a significant enhancement in the interaction time of the light in the medium for the coupled (green) case compared with the uncoupled (violet) case. Nearly three orders of magnitude more light is still trapped in the powder after 10 ns when it is coupled via a hole in the surface. Diffusion theory (cyan and gold) fits with good agreement. (*I*) The average dwell time, calculated from the temporal profile, scales with the hole depth. Here, diffusion theory assumes a 0.7-mm optical collection radius from the sample, and $\mu_a = 10^{-4}$ mm^{-1}. We see that, as the holes become deeper, less light is lost via the hole, and the measured value approaches theory.

axial thickness of the scattering medium, with a prediction that the transmittance of a 1-cm-thick sample will increase by only 19% after reducing the thickness by 350 μm. The same theory predicts that injecting the light 350 μm beneath the surface of the 1-cm-thick sample will enhance the transmittance by over 160 times.

The interaction time of light within the medium is also directly related to the coupling efficiency. This interaction time was observed through time-correlated single-photon-counting measurements (50-ps resolution, SPC-150; Becker & Hickl) of the backscattered intensity as a function of time, as shown in Fig. 3*H* (normalized by peak photon count). From the normalized time domain picture we see that, when the light is focused into the microscopic hole, the decay time of the light is drastically increased. After 10 ns from the arrival of the incident pulse, nearly three orders of magnitude more light is still present in the sample with a hole in it compared with that without a hole.

From optical diffusion theory (*Materials and Methods*), the temporal decay curve of light backscattered from a scattering sample with incident light injected at a depth, h, is described as

$$P(t) = \frac{c}{\sqrt{4\pi Dct}} e^{-\mu_a ct}\left[1 - e^{-\frac{R^2}{4Dct}}\right] \times \left[e^{-\frac{(l_t+h)^2}{4Dct}} - e^{-\frac{(2L_s+l_t+h)^2}{4Dct}}\right], \quad [1]$$

where c is the speed of light, $D = l_t/3$ is the diffusion coefficient, l_t is the transport mean free path, μ_a is the absorption coefficient, R is the detector radius, L_s is the distance used in the extrapolated zero-boundary approximation (31), and t is the time after the arrival of the pulse. Consideration of the detector radius is required because light emitted from the sample farther from the injection point likely has a longer dwell time, and not all backscattered light was collected. The effective injection depth, h, is related to the depth of the hole, and includes a geometrical factor related to the shape of the hole. Leakage of light back through the narrow and deep holes is assumed to be small. In Fig. 3*H*, this curve is compared with data for cases with ($h = 325$ μm) and without ($h = 0$) an engineered interface. Here, fitting parameters are used to adjust for normalization and location of $t = 0$. As predicted, the interaction time scales with hole depth. This finding is further verified by calculating and measuring the average dwell time of the light in the material.

The average time that the scattered light dwells inside the material is calculated using $\langle t\rangle = \int tP(t)dt / \int P(t)dt$, where $P(t)$ is the optical power emitted from the sample as a function of time. This dwell time was measured using time-correlated single-photon counting for samples with different hole depths, and is shown in Fig. 3*I*. The values predicted by diffusion theory are also shown. For shallow holes, the observed dwell times dip below the theory curve; this is because the theoretical assumption that no light leaks back out of the hole is a poor approximation

Downloaded at Palestinian Territory, occupied on December 11, 2021
PHYSICS
APPLIED BIOLOGICAL SCIENCES
www.manaraa.com

for shallow holes. As the hole depth increases, however, this assumption becomes more valid, and the measured dwell time approaches theory. It is important to point out that, by coupling light into the scattering medium via the laser-ablated holes, the dwell time increases from less than 50 ps to 750 ps, more than an order of magnitude enhancement.

Discussion

In summary, we have experimentally demonstrated a drastic increase in the coupling of light into a turbid material, as evident by the increased interaction time and spatial diffusion of laser light within the material. In particular, we have shown over an order of magnitude increase in optical dwell time, and over two orders of magnitude more light penetrating a 1-cm-thick sample. This increase was achieved by ablating a microscopic hole into the optical interface of a material and focusing light into the hole. Compared with diffusion theory, this finding suggests that, as the depth of the narrow hole deepens, the coupling will increase and the amount of light leakage back out of the hole will become negligible. These results were demonstrated for a homogeneous, highly scattering material, but we expect similar effects to be observed within nonhomogeneous media.

Many significant consequences result from this technique. First, the increased dwell time and diffusion distance will enhance the interaction of light with chemicals contained within the scattering medium. Optical signal generated from this interaction (i.e., Raman scattering, fluorescence, etc.) will be likewise enhanced, making it possible to achieve more-sensitive optical measurements in the presence of scattering. Second, the extended penetration depth will not only allow us to probe deeper into a scattering medium for detection purposes, it will also allow us to deliver more optical energy through scattering media (such as tissue, bone, containers, etc.) for medical (9) or defense purposes.

Materials and Methods

Sample Preparation. A sample of highly scattering material is constructed by packing barium sulfate ($BaSO_4$) powder (243353; Sigma-Aldrich) into a 1-inch-diameter lens tube (SM1L10; Thorlabs) with lengths of either 2.5 cm or 1 cm. Barium sulfate has a transport mean free path of 1.2 μm ($\mu_t = 833.2\ mm^{-1}$) as measured by coherent backscattering (32); therefore, these sample thicknesses correspond to 10^4 transport mean free paths. The scattering coefficient and anisotropy parameter of $BaSO_4$, calculated from Mie theory, are $\mu_s = 2{,}083\ mm^{-1}$ and $g = 0.6$, respectively. A hole is ablated in the surface of the sample by focusing 6-ps-long laser pulses (532 nm, APL-X; Attodyne) onto the surface of the powder with a 50-mm lens (AC254-050-A-ML; Thorlabs). The pulse energy for ablation was measured to be 35 μJ per pulse. Because the depth of ablation will saturate (33), the hole reaches a stable depth after a large number of pulses. This depth as a function of the number of ablation pulses was measured via OCT, and is shown in Fig. S1.

OCT. To measure the depth of the hole, we used an OCT system. This system can provide nondestructive morphological images of optical scattering media at depths of 1 mm to 2 mm with high-resolution imaging. The axial resolution of OCT is a function of the light source coherence length. The super-luminescent diode source used here had a center wavelength of 830 nm with a full-width at half maximum of 40 nm, yielding an axial resolution of 7.6 μm. The lateral resolution is a function of the focal spot on the sample, which, in this case, was 6 μm. These high resolutions allow us to acquire a topographical image of the hole. Fig. 2*A* shows an OCT cross-sectional image of a hole in this material ablated with 250 laser pulses. The hole is ∼300 μm deep. We scanned the entire hole, and Fig. 2*B* shows the rendered OCT volume image. The 3D volume clearly shows the conical shape of the hole.

To measure the depth of the hole as a function of the number of laser pulses, an array of 12 holes was ablated into a 1-cm-thick sample of packed $BaSO_4$ using a different number of pulses for each hole. Each hole was separated from its neighbors by about 2 mm. This sample was then imaged using the OCT system. The cross-section of each hole is shown in Fig. S2, and the measured hole depths as a function of the number of ablation pulses are shown in Fig. S1. A curve was fit to these data points to calibrate the hole depth versus the number of ablation pulses for the system, as is also shown in Fig. S1. The values from this calibration curve were used in Fig. 3*I*, which shows the dwell time measurements as a function of hole depth.

Experimental Setup. The experimental setup for ablation, imaging of the powder, and time-correlated single-photon counting is shown in Fig. 4. A picosecond laser (532 nm, APL-X; Attodyne) was used both to ablate the hole and for all measurements except OCT. The beam is first expanded by a factor of 5 using two lenses in a telescope configuration. It is then focused onto the sample with a 50-mm achromatic lens (AC254-050-A-ML; Thorlabs). This same lens also collects the scattered light in the backward direction. Although the hole was ablated in the sample with laser pulse energy at 35 μJ per pulse, the measurements were made with the laser pulse energy tuned down to 150 nJ per pulse. Thus, measurements were acquired in a regime where ablation would not continue to occur.

The images of the backscattered light were acquired by relaying the image of the sample surface with lenses [BPX070 ($f = 100$ mm), AC254-035-A-ML ($f = 35$ mm), and AC254-045-A-ML ($f = 45$ mm); Thorlabs] to a CCD (CGE-B013-U; Mightex) as shown in Fig. 4. A glass slide and mirror (PF10-03-P01; Thorlabs) were used to collect and direct the backscattered light with minimal disruption to the incident laser light. In this case, the flip mirror (FM90; Thorlabs) (Fig. 4) was opened to let the light enter the CCD. Images of the backscattered light from the sample were acquired for samples with and without a hole ablated in the surface. Furthermore, a hypodermic needle (250; Monoject) was inserted into the intermediate image plane to block the focus of the laser, allowing us to more clearly see the increased diffusion radius of light emitted from the sample. These images were acquired for a 2.5-cm-thick sample.

Measurements of the light transmitted through a 1-cm-thick sample were acquired by a large area photodiode (DET100A; Thorlabs) placed at the back side of the sample, with a 25.4-mm-focal-length lens (LA1951-ML; Thorlabs) to collect the transmitted light onto the photodiode detector. The intensity of the transmitted light was then measured with the incident light focused into the hole or focused onto the surface about 1 mm away from the hole. This coupling and uncoupling of the laser into the hole was achieved by translating the sample, lens, and photodiode in a direction perpendicular to the beam. Thus, the ratio of the transmitted light through the sample when the incident light is coupled into vs. uncoupled from the hole was measured to be over 200 times. Furthermore, this effect was imaged by removing the photodiode and lens and placing a CCD with two imaging lenses of focal length 300 mm (AC254-300-A-ML; Thorlabs) and 45 mm (AC254-045-A-ML; Thorlabs) behind the sample. These images are shown in Fig. 3 *F* and *G*.

Time-Correlated Single-Photon Counting. Temporal measurements of the backscattered light were measured via time-correlated single-photon counting. In this case, roughly 1.16% of the backscattered light was collected again with the focusing lens ($f = 50$ mm), glass slide, and mirror (PF10-03-P01;

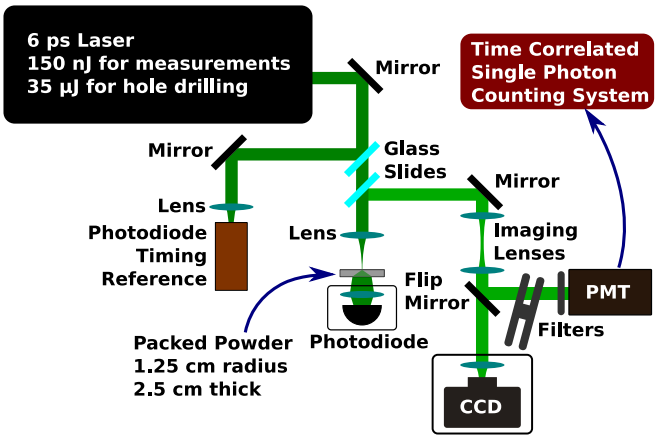

Fig. 4. Experimental setup. Six-picosecond laser pulses are used to ablate a microscopic hole in a packed slab of highly scattering powder. A photomultiplier tube is used as input to a time-correlated single-photon-counting system to measure the decay of the light scattering off of the powder. A CCD also images the spatial scattering in the sample, and a large area photodiode measures the amount of light transmitted through the sample.

Downloaded at Palestinian Territory, occupied on December 11, 2021
www.manaraa.com

Thorlabs). The imaging lenses shown in Fig. 4 were removed, and the flip mirror (FM90; Thorlabs) was closed so that the scattered light was directed into a multichannel plate photomultiplier tube (R3809U-50; Hamamatsu). With the laser running at a 1-MHz repetition rate, the detection rate of the photomultiplier tube was kept between 10 kHz and 15 kHz, using various combinations of neutral density filters (5215; Newport; and NDK01/NEK01; Thorlabs). This limiting of the detection rate to one photon for every 66 to 100 laser pulses was to avoid biased or uneven temporal distribution of the counted photons. The timing of the signal from the photomultiplier tube was measured with respect to a reference pulse by a time-correlated single-photon-counting module (50-ps resolution, SPC-150; Becker & Hickl). The reference pulse was taken from the laser beam before the scattering material with a glass slide, and collected onto a photodiode module (PHD-400; Becker & Hickl). After collecting a sufficient number of signals, the time of arrival for each signal is binned to create a statistical representation of the scattered light as a function of time.

Because of the sensitivity of the time-correlated single-photon-counting method to small changes in the setup parameters, such as the photomultiplier voltage and the threshold values for both the signal and reference pulse, these parameters were first determined by calibration to the fluorescent lifetime of Rhodamine 6G in water (2 μM concentration). Once calibrated, we used the same parameters for all other measurements. We also used the neutral density filters to ensure that the photon rate of the signal stayed nearly the same. With our calibrated system, we measured the lifetime of Rhodamine 6G in water to be 4.1 ns, which is comparable to the previously reported value of 4.08 ns (34).

The time of arrival of the scattered light from a sample with and without a hole is shown in Fig. 3*H*. The signal for the sample with a hole was acquired with a collection time of 6 min. The signal from the sample without a hole required 60 min of collection time to realize good signal to noise at longer times. Careful shielding of the photomultiplier tube was critical to remove the light from any stray reflections in the room; however, a couple very weak reflections ($< 10^{-4}$) are still visible in the signal from the sample without a hole at 4 ns and 12 ns after the pulse arrives.

For the measurement of the average dwell time, 2-min acquisitions were used to measure the temporal signal as a function of hole depth. The shorter collection time allowed for faster acquisition of the data with very little effect upon the dwell time measurement; this is because of the orders of magnitude falloff soon after the pulse arrives and the nature of the time-weighted integral ($\int tP(t)dt$). Different hole depths were ablated by controlling the number of ablation pulses used, and the depths were calibrated using OCT as previously discussed.

Theoretical Model: Interaction Time. The dynamics of the backscattered light are modeled with the optical diffusion equation for radiative transport (35).

$$\frac{1}{c}\frac{\partial\Phi(\boldsymbol{r},t)}{\partial t}+\mu_a\Phi(\boldsymbol{r},t)-D\nabla^2\Phi(\boldsymbol{r},t)=S(\boldsymbol{r},t). \quad [2]$$

Here c is the speed of light, $\Phi(\boldsymbol{r},t)$ is the optical fluence rate, μ_a is the absorption coefficient, $D=l_t/3$ is the diffusion coefficient, and $S(\boldsymbol{r},t)$ is a source term. Also, $l_t=1/\mu_t$ is the transport mean free path, where μ_t is the extinction coefficient with anisotropy parameter $g=\langle\cos(\theta)\rangle$ and is defined as $\mu_t=(1-g)\mu_s+\mu_a$, for scattering coefficient μ_s. This equation is solved using the Green function for a point light source (31) and the method of images. Here, we assume a point light source is located at $\boldsymbol{r'}=\langle 0,0,l_t+h\rangle$, where h denotes the injection depth of the light. Using a point source assumes that all of the injected light enters the material at the same depth. A more rigorous approach would model the injected light as an extended source, based upon the geometry of the hole. However, there is an equivalent depth, $h=\eta h_0$, at which a point source can be placed to approximate the more rigorous extended source. Here, h_0 is the depth of the hole, and the geometrical factor is $0\le\eta\le 1$. Thus, for simplicity, we assume that the only effect of the hole is to inject the light into the scattering slab at this equivalent depth of (l_t+h). This approach still neglects any light that escapes back through the hole, assuming it is small for deep and narrow holes.

The optical power of the light that exits the medium to the surface $[\Phi(z=0,t)]$ is found by integrating the Green function solution over the detector area (circle with radius R), yielding Eq. **1**. Here, L_s is the distance used in the extrapolated zero-boundary approximation (31), at which the fluence rate, $\Phi(\boldsymbol{r},t)$, is equal to zero. This equation is compared with the data in Fig. 3*H* using a scaling parameter and slight temporal offset as fitting parameters to adjust for normalization and location of $t=0$. Here, we assumed a collection radius of 0.7 mm, $\mu_a=10^{-4}$ mm^{-1}, and an equivalent hole depth, $h=325$ μm, for the coupled case. For the uncoupled case, the hole depth is set to zero.

It is also intuitive to see that, for long times $[t\gg R^2/(4Dc)$ and $t\gg h^2/(4Dc)]$, Eq. **1** simplifies to

$$P(t)\approx\frac{cR^2L_s(L_s+l_t+h)}{8\sqrt{\pi}}\frac{1}{[Dct]^{5/2}}e^{-\mu_a ct}. \quad [3]$$

Thus, the interaction time of light with the material should scale with hole depth; this is measured by computing the average dwell time of the light in the medium.

From the integration of Eq. **1**, the dwell time of light in the scattering medium, $\langle t\rangle=\int tP(t)dt/\int P(t)dt$, is found to have the form

$$\langle t\rangle=\frac{1}{2\mu_a c}\left[1+\frac{k_0e^{-k_0}-k_1e^{-k_1}-k_2e^{-k_2}+k_3e^{-k_3}}{e^{-k_0}-e^{-k_1}-e^{-k_2}+e^{-k_3}}\right], \quad [4]$$

where the coefficients, k_j, are equal to

$$\begin{aligned}k_0&=\sqrt{\frac{\mu_a}{D}}(l_t+h)\\ k_1&=\sqrt{\frac{\mu_a}{D}}(2L_s+l_t+h)\\ k_2&=\sqrt{\frac{\mu_a}{D}}\sqrt{(l_t+h)^2+R^2}\\ k_3&=\sqrt{\frac{\mu_a}{D}}\sqrt{(2L_s+l_t+h)^2+R^2}.\end{aligned} \quad [5]$$

Although Eq. **4** is plotted in Fig. 3*I*, it is intuitive to see that, for $h\ll R$ (as well as $h\gg l_t$ and $h\gg L_s$), the dwell time has a linear dependence upon h. In this regime, Eq. **4** simplifies to

$$\langle t\rangle\approx\frac{h+l_t+L_s}{2c\sqrt{D\mu_a}}\left(1-e^{-R\sqrt{\frac{\mu_a}{D}}}\right). \quad [6]$$

We note here the dependence of the dwell time upon the scattering properties. In particular, as the diffusion coefficient, D, decreases (i.e., increased scattering coefficient), the dwell time increases. Thus, for a given hole depth, the dwell time is longer for media with stronger scattering. The enhancement due to an effective hole depth of $h=350$ μm is shown in Fig. S3 as a function of transport mean free path.

Theoretical Model: Enhanced Transmittance. The optical transmittance through a scattering sample is modeled for a slab of finite thickness with an infinite series of dipole sources. Here, keeping terms from the first four dipoles, as calculated in ref. 30, with extension to include the extrapolated zero-boundary approximation (31), the transmittance is written as

$$T(\rho,d,h,t)=\frac{1}{2}(4\pi Dc)^{-3/2}t^{-5/2}e^{-\mu_a ct}e^{-\frac{\rho^2}{4Dct}}\sum_{n=0}^{N=7}(-1)^n\alpha_n e^{-\frac{\alpha_n^2}{4Dct}}, \quad [7]$$

where d is the thickness of the medium, ρ is the radius from the optical axis, and the α_n coefficients are

$$\begin{aligned}\alpha_0&=d-h-l_t & \alpha_4&=3d-h-l_t+4L_s\\ \alpha_1&=d+h+l_t+2L_s & \alpha_5&=3d+h+l_t+6L_s\\ \alpha_2&=d-h-l_t+2L_s & \alpha_6&=3d-h-l_t+6L_s\\ \alpha_3&=d+h+l_t+4L_s & \alpha_7&=3d+h+l_t+8L_s.\end{aligned} \quad [8]$$

Integration over the transverse direction and time $[\int_0^\infty\int_0^{2\pi}\int_0^R T(\rho,d,t)\rho\,d\rho\,d\phi\,dt]$ yields the total transmittance as a function of sample thickness (d), optical injection depth (h), and detector radius (R).

$$T(d,h,R)=\frac{1}{2}\sum_{n=0}^{N=7}(-1)^n\left[e^{-\sqrt{\frac{\mu_a}{D}}\alpha_n}-\frac{\alpha_n}{\sqrt{R^2+\alpha_n^2}}e^{-\sqrt{\frac{\mu_a}{D}(R^2+\alpha_n^2)}}\right]. \quad [9]$$

From this equation, we find that, by placing the source 0.35 mm below the surface of a $d=10$-mm-thick sample with $\mu_a=10^{-4}$ mm^{-1} and $\mu_t=833.2$ mm^{-1}, the transmittance is enhanced by a factor of over 160. In comparison, reducing the thickness to $d=9.65$ mm with $h=0$ will only increase the transmitted light by 19%.

The relationship between transmittance and the diffusion coefficient is less obvious in this case than in the case of dwell time. However, plotting Eq. **9** (Fig. S3) as a function of l_t, for $h=350$ μm and $d=10$ mm, we see that the enhancement of transmittance due to the microscopic interface is also greater for samples with a stronger scattering coefficient.

ACKNOWLEDGMENTS. This research was supported in part by the National Science Foundation [Chemical, Bioengineering, Environmental,

Downloaded at Palestinian Territory, occupied on December 11, 2021
PHYSICS
APPLIED BIOLOGICAL SCIENCES
www.manaraa.com

and Transport Systems Award 1250363, Division of Biological Infrastructure Award 1455671, Electrical, Communications, and Cyber Systems (ECCS) Award 1509268, and Grant ECCS-1509361], the Robert A. Welch Foundation (Grant A-1261), the Office of Naval Research (Grants N00014-16-1-3054 and N00014-13-1-0649), and the US Department of Defense (Grant FA9550-15-1-0517). J.V.T. has been supported by the Herman F. Heep and Minnie Belle Heep Texas A&M University Endowed Fund held/administered by the Texas A&M Foundation. B.H.H. acknowledges a graduate fellowship from the Department of Defense Science, Mathematics and Research for Transformation fellowship program.

1. Czarnik AW (1998) A sense for landmines. *Nature* 394:417–418.
2. Geng Y, et al. (2015) Unambiguous detection of nitrated explosive vapours by fluorescence quenching of dendrimer films. *Nat Commun* 6:8240.
3. Ben-Jaber S, et al. (2016) Photo-induced enhanced Raman spectroscopy for universal ultra-trace detection of explosives, pollutants and biomolecules. *Nat Commun* 7:12189.
4. Hokr BH, et al. (2014) Single-shot stand-off chemical identification of powders using random Raman lasing. *Proc Natl Acad Sci USA* 111:12320–12324.
5. Battersby BJ, Lawrie GA, Johnston APR, Trau M (2002) Optical barcoding of colloidal suspensions: Applications in genomics, proteomics and drug discovery. *Chem Commun (Camb)* 14:1435–1441.
6. Extance A (2015) Laser weapons get real. *Nature* 521:408–410.
7. Sathyendranath S, et al. (1991) Estimation of new production in the ocean by compound remote sensing. *Nature* 353:129–133.
8. Backman V, et al. (2000) Detection of preinvasive cancer cells. *Nature* 406:35–36.
9. Sugiura T, et al. (2015) Photothermal therapy of tumors in lymph nodes using gold nanorods and near-infrared laser light with controlled surface cooling. *Nano Res* 8:3842–3852.
10. Kong K, Kendall C, Stone N, Notingher I (2015) Raman spectroscopy for medical diagnostics—From in-vitro biofluid assays to in-vivo cancer detection. *Adv Drug Deliv Rev* 89:121–134.
11. Hokr BH, et al. (2014) Bright emission from a random Raman laser. *Nat Commun* 5:4356.
12. Harrison DJ, et al. (1993) Micromachining a miniaturized capillary electrophoresis-based chemical analysis system on a chip. *Science* 261:895–897.
13. Sarma R, Yamilov A, Petrenko S, Bromberg Y, Cao H (2016) Control of energy density inside disordered medium by coupling to open or closed channels. *Phys Rev Lett* 117:086803.
14. Vynck K, Burresi M, Riboli F, Wiersma DS (2012) Photon management in two-dimensional disordered media. *Nat Mater* 11:1017–1022.
15. Wiersma DS (2013) Disordered photonics. *Nat Photon* 7:188–196.
16. Chandrasekhar S (1960) *Radiative Transfer* (Dover, New York), pp 1–416.
17. Day JCC, Stone N (2013) A subcutaneous Raman needle probe. *Appl Spectros* 67: 349–354.
18. Vellekoop IM, Mosk AP (2007) Focusing coherent light through opaque strongly scattering media. *Opt Lett* 32:2309–2311.
19. Mosk AP, Lagendijk A, Lerosey G, Fink M (2012) Controlling waves in space and time for imaging and focusing in complex media. *Nat Photon* 6:283–292.
20. Thompson JV, Throckmorton GA, Hokr BH, Yakovlev VV (2016) Wavefront shaping enhanced Raman scattering in a turbid medium. *Opt Lett* 41:1769–1772.
21. Ojambati OS, Yilmaz H, Lagendijk A, Mosk AP, Vos WL (2016) Selective coupling of optical energy into the fundamental diffusion mode of a scattering medium. *New J Phys* 18:0432032.
22. Vellekoop IM, Mosk AP (2008) Universal optimal transmission of light through disordered materials. *Phys Rev Lett* 101:1–4.
23. Popoff S, Lerosey G, Fink M, Boccara AC, Gigan S (2010) Image transmission through an opaque material. *Nat Commun* 1:81.
24. Vellekoop IM, Mosk AP (2008) Phase control algorithms for focusing light through turbid media. *Opt Commun* 281:3071–3080.
25. Thompson J, Hokr B, Yakovlev V (2016) Optimization of focusing through scattering media using the continuous sequential algorithm. *J Mod Opt* 63:80–84.
26. Popoff SM, et al. (2010) Measuring the transmission matrix in optics: An approach to the study and control of light propagation in disordered media. *Phys Rev Lett* 104: 1–4.
27. Sarma R, Yamilov A, Liew SF, Guy M, Cao H (2015) Control of mesoscopic transport by modifying transmission channels in opaque media. *Phys Rev B Condens Matter Mater Phys* 92:1–10.
28. Xu X, Liu H, Wang LV (2011) Time-reversed ultrasonically encoded optical focusing into scattering media. *Nat Photon* 5:154–157.
29. Ebbesen T, Lezec HJ, Ghaemi HF, Thio T, Wolff PA (1998) Extraordinary optical transmission through sub-wavelength hole arrays. *Nature* 86:1114–1117.
30. Patterson MS, Chance B, Wilson BC (1989) Time resolved reflectance and transmittance for the non-invasive measurement of tissue optical properties. *Appl Opt* 28:2331–2336.
31. Haskell RC, et al. (1994) Boundary conditions for the diffusion equation in radiative transfer. *J Opt Soc Am A Opt Image Sci Vis* 11:2727–2741.
32. Cao H, et al. (1999) Random laser action in semiconductor powder. *Phys Rev Lett* 82:2278–2281.
33. Chuang MC, Tam AC (1989) On the saturation effect in the picosecond near ultraviolet laser ablation of polymide. *J Appl Phys* 65:2591–2595.
34. Magde D, Rojas GE, Seybold PG (1999) Solvent dependence of the fluorescence lifetimes of xanthene dyes. *Photochem Photobiol* 70:737–744.
35. Welch AJ, Van Gemert MJC (2011) *Optical-Thermal Response of Laser-Irradiated Tissue* (Springer, New York), 2nd Ed, pp 1–958.

Downloaded at Palestinian Territory, occupied on December 11, 2021

www.manaraa.com